Nonlinear Dyn (2015) 79:1411–1424
DOI 10.1007/s11071-014-1750-1

ORIGINAL PAPER

Effect of the lower boundary of reinjection and noise in Type-II intermittency

Sergio Elaskar · Ezequiel del Río · Gustavo Krause · Andrea Costa

Received: 26 May 2014 / Accepted: 10 October 2014 / Published online: 25 October 2014

Abstract We implement a recent methodology to study type-II intermittency considering different values of the lower boundary of reinjection (LBR) and the noise intensity. With this approach, analytical expressions for the reinjection probability density (RPD) are accurately obtained. The proposed RPD has a piecewise definition addressing the different reinjection mechanisms appearing in the system depending on the LBR value and the noise intensity. Also, the new probability density of the laminar lengths is calculated. When LBR $\neq 0$, the noisy probability density of the laminar lengths presents a cutoff, which disappears for noise strength different to zero. The theoretical results are verified with numerical simulations.

Keywords Type-II intermittency · Noise · Chaos

S. Elaskar · G. Krause (✉)
Dpto. de Aeronáutica Facultad de Ciencias Exactas, Físicas y Naturales Universidad Nacional de Córdoba – CONICET, Córdoba, Argentina
e-mail: gustavojavierkrause@gmail.com

S. Elaskar
e-mail: selaskar@efn.uncor.edu

E. del Río
Departamento de Física Aplicada, ETSIA, Universidad Politécnica de Madrid, Madrid, Spain

A. Costa
Instituto de Astronomía Teórica y Experimental, IATE-CONICET, Argentina

1 Introduction

Chaotic intermittency is a route to chaos where dynamical systems have transitions between regular (or laminar) phases and chaotic bursts (or non regular phases). The laminar phases are regions of pseudo-equilibrium and/or pseudo-periodic solutions, and the bursts ones are regions where the evolution is chaotic. Pomeau and Manneville introduced the concept of intermittency in [1,2]. Traditionally, intermittency is classified into three different types called I, II and III [3–5] according to the Floquet multipliers of the system or to the eigenvalues in the local Poincaré map. However, more recent studies have extended the classification to other types of intermittencies such as type V, X, on-off, eyelet and ring [6–11]. A more general case of on-off intermitency is the so-called in-out intermitency. Both types of intermittencies were observed in coupled oscillators. A complete review of on-off and in-out intermittencies can be found in [12].

In type-I, type-II and type-III intermittency phenomena, when a control parameter exceeds a threshold value, an explosive bifurcation [4] leads to a change of the system behavior toward a chaotic motion that converges into a larger attractor. In all cases, a fixed point of the local Poincaré map becomes unstable or even vanishes for some values of the control parameter ε. Intermittency has been observed in several physical studies such as Lorenz system, Rayleigh–Bénard convection, forced nonlinear oscillators, plasma physics, electronic circuits, turbulent flows [13–21]. Also, inter-

mittency was used to describe the behavior of economy and medicine systems [22–24]. The accurate description of intermittency helps to improve the knowledge about these phenomena. On the other hand, the proper characterization of intermittency has great importance for systems whose exact governing equations are totally or partially unknown.

Type-II intermittency was found in a driven double scroll circuit as a consequence of a global bifurcation scenario for T^2 torus breakdown [25,26]. Also, characteristic relations for type-II intermittency were studied in [27]. The noise effect on the intermittency phenomenon was studied using renormalization group analysis or by using the Fokker-Plank equation [28–30].

Intermittency may be studied using Poincaré maps [3,4]. Two main features characterize chaotic intermittency: (1) a specific local map and (2) a reinjection mechanism. Type-II intermittency departures from a subcritical Hopf bifurcation or a Naimark-Sacker bifurcation [4,31], then two complex-conjugate Floquet multipliers of the system or two complex-conjugate eigenvalues of the local Poincaré map must move away from the unit circle and a stable fixed point of the system becomes unstable. The local Poincaré map for type-II intermittency can be written as $x_{n+1} = (1+\varepsilon)x_n + a\ x_n^3$, where the control parameter ε and the coefficient a are larger than zero [32]. The reinjection mechanism maps back the system into the local regular or laminar zone from the chaotic one. This mechanism is described by means of a probability function called reinjection probability density (RPD) which gives the probability that trajectories are reinjected into the laminar zone, close to the unstable fixed point. This function depends on the nonlinear dynamics of the system itself and can lead to a broad range of different behavior.

The accurate evaluation of the RPD function is extremely important to correctly describe the chaotic intermittency phenomenon. Still, the experimental or numerical evaluation of the RPD function is not a simple task due to the huge amount of data needed. Moreover, the statistical fluctuations induced in the numerical computations and the experimental measurements are difficult to estimate. The usual approach was to consider a uniform reinjection using a constant RPD function. Other implemented approaches built the RPD using peculiar features of the nonlinear processes. Nevertheless, these RPD functions cannot be successfully applied to other nonlinear systems. Two examples are given in [30,33]: to investigate the effect of noise in type-I intermittency, it is assumed that the reinjection is localized in a fixed point [33]; and for type-III intermittency in an electronic circuit, the RPD was considered proportional to $1/\sqrt{x-\Delta}$ in [30].

A more general methodology to obtain the RPD, which includes the uniform reinjection as a particular case, was introduced [32,34–40]. In this paper, we implement this methodology to describe the type-II intermittency. The reinjection processes considering noise effect and a lower boundary of reinjection different to zero (LBR $\neq 0$) are analyzed. Several new theoretical noisy RPD functions that are differentiable by segments are obtained. The new noisy RPD are compared with numerical results showing a good agreement.

2 Evaluation of the statistical properties

In this section, a brief description of the theoretical framework that accounts for a wide class of dynamical systems exhibiting intermittency is presented. To describe the new formulation, a general one-dimensional map: $x_{n+1} = F(x_n)$ is considered. The RPD function, denoted here by $\phi(x)$, determines the probability that trajectories are reinjected into a point x inside the laminar interval. The RPD specifies the statistical behavior of the reinjection trajectories, which depend on the specific form of $F(x)$ [3,4]. In this paper, the RPD is not directly obtained from the numerical data. Instead, we use a methodology developed in last years to deal with intermittency [32,34–40]. Thus, the main expression for a more general formulation, is given by a function $M(x)$

$$M(x) = \begin{cases} \dfrac{\int_{x_s}^{x} \tau\phi(\tau)\,\mathrm{d}\tau}{\int_{x_s}^{x} \phi(\tau)\,\mathrm{d}\tau}, & \text{if } \int_{x_s}^{x} \phi(\tau)\,\mathrm{d}\tau \neq 0, \\ 0, & \text{otherwise,} \end{cases} \tag{1}$$

where τ represents the reinjected points around the unstable fixed point, and x_s is the closest reinjection point to the unstable fixed point, i.e., the lower boundary of reinjection point. An experimental evidence of the LBR effect for intermittent phenomenon was presented in [13].

Therefore, the laminar interval is given by $x_s \leq x \leq c$. Where c is a constant verifying $c > 0$ which specifies the upper limit of the laminar region around the unstable fixed point x_0. Accordingly, the laminar zone

of intermittency is defined by $[x_s, x_0 + c]$. In previous type-II intermittency works, $x_s \equiv x_0$ (LBR = 0) was adopted [32,35]. Here, $x_s \neq x_0$ will be considered.

$M(x)$ is an auxiliary function used to evaluate the RPD. Since, $M(x)$ is a quotient between two integrals, it softens the fluctuations of the experimental or numerical data used to construct it [32,34–40]. On the other hand, function $M(x)$ corresponds to the average over the reinjection points in the laminar interval; hence, its numerical estimation is more robust than the direct evaluation of the function $\phi(x)$. In addition, the calculation of $M(x)$ from the data series is very simple:

$$M(x) \approx \frac{1}{N}\sum_{j=1}^{N} x_j, \tag{2}$$

where the data set (reinjection points) $\{x_j\}_{j=1}^{N}$ must be sorted from the lowest to the highest, i.e., $x_j \leq x_{j+1}$. For a wide class of maps exhibiting type-I, type-II and type-III intermittencies, it was found that the function $M(x)$ satisfies a linear approximation [32,34–36,38]:

$$M(x) = \begin{cases} m(x - x_s) + x_s, & \text{if } x_s \leq x \leq c, \\ 0, & \text{otherwise}, \end{cases} \tag{3}$$

where the slope $m \in (0, 1)$ is a free parameter defined by the nonlinear map, and it governs the reinjection process. Therefore, the function $M(x)$ satisfies $M(x) \leq x$ according to the definition given by Eq. (2): an average value over the reinjected points inside the interval $[x_s, x]$. Introducing Eq. (3) in Eq. (1), the corresponding RPD function results [34,36]:

$$\phi(x) = \lambda(x - x_s)^{\alpha}, \quad \text{with } \alpha = \frac{2m - 1}{1 - m}, \tag{4}$$

where λ is a normalization parameter. Note that for $m = 1/2\,(\alpha = 0)$, the uniform RPD is recovered, i.e., uniform reinjection is obtained as a particular case of the new formulation.

3 Type-II intermittency

A formulation can be applied to a one-dimensional map with type-II intermittency following [32]. The implemented map is:

$$x_{n+1} = \begin{cases} (1 + \varepsilon)x_n + a x_n^p, & x_n \leq x_r, \\ x_s + (1 - x_s)\left[\dfrac{x_n - x_r}{1 - x_r}\right]^{\gamma}, & x_n > x_r, \end{cases} \tag{5}$$

where x_r is defined by $(1 + \varepsilon)x_r + a x_r^p = 1$, and ε is the control parameter. The map, which allows to analyze different types of reinjection mechanism, has the fixed point $x = 0$ at the origin, which is stable for $-2 < \varepsilon < 0$. When $\varepsilon > 0$, the fixed point becomes unstable and type-II intermittency is generated. The iteration procedure—governed by the parameter ε and the exponent p—gives increasing values of x_n generated from an initial one, close to the origin. A chaotic burst occurs if x_n becomes larger than x_r and ends when the trajectory is reinjected into a point in the laminar zone. Then, a new iterative process –governed by ε and p—will be developed producing larger values of the new successive iterative points. Note that γ drives the reinjection mechanism, whereas p and ε determine the laminar phase duration; and if there is not LBR, $x_s = 0$, the laminar zone includes the unstable fixed point. If $p = 3$, the local Poincaré map is of type-II intermittency.

The function $M(x)$ was numerically evaluated obtaining a linear form $M(x) = m(x - x_s) + x_s$ for different values of γ and ε. Hence, the RPD function can be expressed by Eq. (4) with $\lambda = (\alpha + 1)/(c - x_s)^{\alpha+1}$. Also, $\phi(x)$ can depart from a uniform reinjection, e.g., $\lim_{x\to 0}\phi(x)$ is infinity when $0 < m < 1/2$ and zero, when $1/2 < m < 1$.

The function $M(x)$ is only defined by the parameter m, and it is easier to obtain among a huge amount of data than the complete RPD function. Note that $M(x)$ satisfies $M(x_s) = x_s$, then, in addition, it allows to evaluate the LBR.

Inside the laminar zone, with $\varepsilon \to 0$, the local map can be approximate by a differential equation [3]:

$$\frac{\mathrm{d}x}{\mathrm{d}l} = \varepsilon x + a x^p. \tag{6}$$

Integrating this expression, the laminar length for each reinjection point, x_{in}, results:

$$\begin{aligned} l(x_{in}, c) &= \int_{x_{in}}^{c} \frac{\mathrm{d}x}{\varepsilon x + a x^p} \\ &= \frac{1}{\varepsilon}\left[\ln\left(\frac{c}{x_{in}}\right) - \frac{1}{p-1}\frac{a c^{(p-1)} + \varepsilon}{a x_{in}^{(p-1)} + \varepsilon}\right]. \end{aligned} \tag{7}$$

The probability density of the laminar lengths, $\phi_l(l)$, is a global property and is related to the reinjection

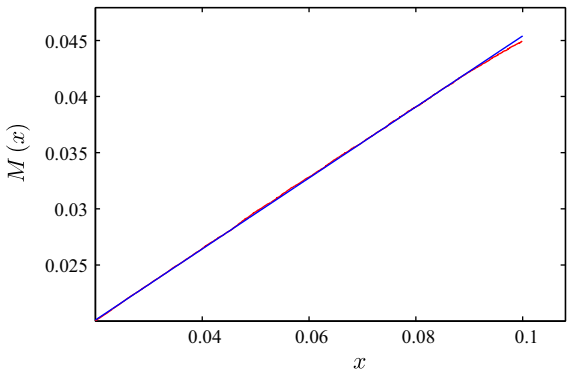

Fig. 1 Function $M(x)$ for map (5). The parameters are $\varepsilon = 0.001$, $c = 0.1$, $x_s = 0.02$, $\gamma = 2$ and $p = 3$. The *red dots* represent the numerical data and the *blue line* is obtained by minimal *square* techniques. (Color figure online)

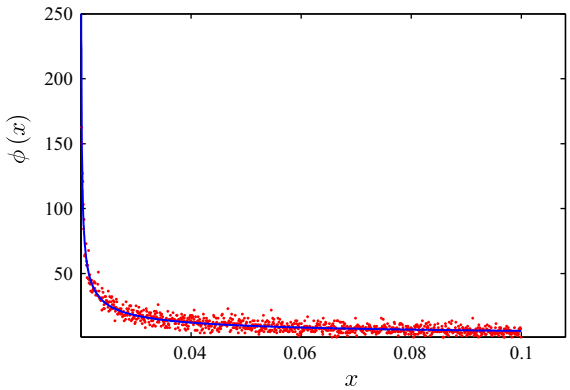

Fig. 2 RPD function for map (5). The parameters are $\varepsilon = 0.001$, $c = 0.1$, $x_s = 0.02$, $\gamma = 2$ and $p = 3$. The *red dots* represent the numerical data and the *blue line* is obtained using Eq. (4). (Color figure online)

probability density function, $\phi(l, c)$, by the expression [32,34]:

$$\phi_l(l, c) = \lambda \left[x(l, c) - x_s\right]^{\alpha} \left[\varepsilon x(l, c) + a x(l, c)^p\right], \tag{8}$$

where $x(l, c)$ is the inverse of $l(x, c)$ given by Eq. (7). Thus, $\phi_l(l, c)$ depends on the global parameter α, and the probability of the laminar length is defined by the slope m of the linear function $M(x)$.

A good agreement between the theoretical results and the numerical data is obtained for different values of γ and ε. Figures 1, 2 and 3 show $M(x)$, $\phi(x)$ and $\phi_l(l)$, respectively, for $\varepsilon = 0.001$, $c = 0.1$, $x_s = 0.02$, $\gamma = 2$ and $p = 3$. These figures were obtained using 10,000 reinjected points.

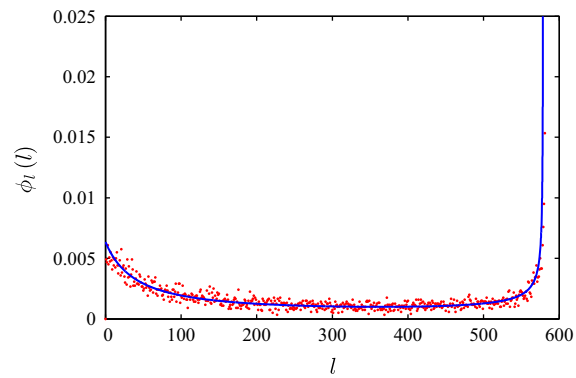

Fig. 3 Probability of laminar lengths for map (5). The parameters are $\varepsilon = 0.001$, $c = 0.1$, $x_s = 0.02$, $\gamma = 2$ and $p = 3$. The *red dots* represent the numerical data and the *blue line* is obtained using Eq. (8). (Color figure online)

From Fig. 1, the slope $m = 0.3147$ ($\alpha = -0.5409$) was obtained. Figure 3 shows the cutoff in the laminar length which is produced by the lower boundary of reinjection, $x_s = 0.02$. For this example, the cutoff is $l_{max} = 581$ (compared with Figure 4 of Ref. [32] where $l_{max} \to \infty$).

Another important property of the intermittent behavior is the average laminar length $\bar{l}$. If m does not depend on ε, it can be written as [32,38]:

$$\bar{l} \approx \frac{1}{a(c - x_s)^{\alpha+1}} \left(\frac{a}{\varepsilon}\right)^{\frac{p-\alpha-2}{p-1}} \frac{\pi}{p-1} \sin^{-1}\left[\frac{\pi(1+\alpha)}{p-1}\right], \tag{9}$$

and the characteristic relation is:

$$\bar{l} \propto \varepsilon^{\frac{\alpha+2-p}{p-1}}. \tag{10}$$

The characteristic relation depends on both: the behavior of the local map around the fixed point given by the parameters p, a and ε, and the global dynamics of the map represented by the parameters α or m. The map (5), in the region where the chaotic dynamic occurs, depends on the exponent γ. Then, the RPD should also depend on γ. Thus, α and m are strongly dependent of γ and are weakly dependent of ε. In [32], a numerical test to evaluate $\bar{l}$ as a function of ε, for several values of γ and $p = 2, 3$, was performed. The results were in good accordance with the theoretical predictions given by Eq. (9).

4 Noise influence

In this section, the influence of noise on the statistical properties of type-II intermittency is studied [35]. As noise affects any natural dynamical system, it will affect the RPD function. In previous studies, it is usually assumed that the noise strength σ is much smaller than ε. Here, a general process where this hypothesis is not necessary is considered. To include the noise the map (5) is transformed into the noisy map:

$$x_{n+1} = \begin{cases} (1+\varepsilon)x_n + a x_n^p + \sigma\xi_n, & x_n \le x_r, \\ x_s + (1-x_s)\left[\dfrac{x_n - x_r}{1-x_r}\right]^\gamma + \sigma\xi_n, & x_n > x_r, \end{cases} \tag{11}$$

where ξ_n is a uniform distributed noise verifying that $\langle \xi_m, \xi_n \rangle = \delta(m-n)$ and $\langle \xi_n \rangle = 0$, with noise strength σ. To keep x_{n+1} in the unit interval the map is modified as:

$$x_{n+1} = \begin{cases} |x_{n+1}|, & \text{if } x_{n+1} \le 0 \\ |x_{n+1}| - 2\bmod(|x_{n+1}|, 1), & \text{if } x_{n+1} > 1. \end{cases} \tag{12}$$

The first condition of Eq. (12) implies that the map is symmetric around the fixed point x_0. If $\sigma = 0$, the previous map (5) is recovered. Figure 4 shows the reinjection mapping into the laminar region. The solid line represents the noiseless trajectory. However, the trajectory for the system (11)–(12), due to noise, will fall in a region enclosed by the dashed lines: the interval l_0.

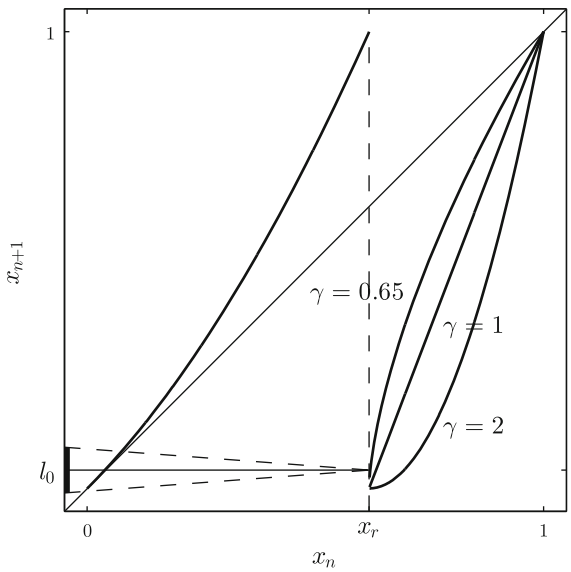

Fig. 4 Map of Eqs. (11)–(12). If $\sigma = 0$, it is equal to map (5)

The presence of noise not only affects the RPD function due to the deviations produced on the reinjection trajectories, but also a new reinjection mechanism can appear when the strength σ is relatively large, as described below. In addition, a parameter such as the LBR can also modify the statistical properties of the reinjection process. When a trajectory has a reinjected point close to the unstable fixed point, the following iterative points increase driven by the parameters ε, a, p and σ until a point, x_n, leaves the laminar interval. If the difference between x'_{n+1} (obtained from (5), without noise) and the laminar boundary c is less or equal than the noise intensity ($x'_{n+1} - c \le \sigma$), the trajectory can return into the laminar interval. This behavior is produced by the noise and is here defined as adjacent reinjection (AR). If there is no noise ($\sigma = 0$), there is no AR. In the following sections, we analyze the noise effect on type-II intermittency considering the influence of the AR mechanisms and the position of the LBR.

4.1 Noisy RPD for LBR = 0 and without AR

In paper [35], we studied the functions $M(x)$ and RPD for type-II intermittency with noise and for the particular case LBR = 0.

In Fig. 5, we show numerical results for the noisy $M(x)$. As for the noiseless case, the function $M(x)$ smooths down the data. However, for the noisy tests, the function $M(x)$ has different behavior on each side of x_c. We call singular points to those points where the behavior of $M(x)$ changes, e.g., x_c. $M(x)$ can be approximated by a piecewise linear function with two slopes. The x_c value is equal to the noise intensity, $x_c = \sigma$. For $x < x_c$, the slope of $M(x)$ approaches $1/2$, as expected for uniform reinjection. For $x > x_c$, the slope of $M(x)$ has a similar value as the noiseless slope. For $\gamma = 0.65$, in the noisy test, the slope is $m \approx 0.61$ and $m \approx 0.60$ in the noiseless case. Thus, in the region $x > x_c$, the noisy RPD (NRPD) must have a similar form to the noiseless RPD function. This is a remarkable property of $M(x)$ because we can obtain the RPD function for the noiseless case by means of a noisy data analysis. Note that even when noise acts on

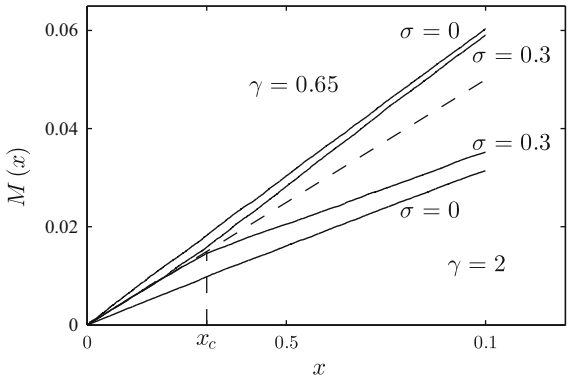

Fig. 5 $M(x)$ from the numerical simulations of the map (11)–(12). The *dashed line* has a $1/2$ slope. The *lines* above the *dashed line* correspond to $\gamma = 0.65$. The same noise strength value is used for the *two lines* below the *dashed one*, corresponding to $\gamma = 2$. For all cases $\varepsilon = 0.001$ is fixed, and $c = 0.1$ and $x_s = 0$

the complete system, it does not modify the slope of $M(x)$ in the region $x > x_c$. Hence, on the right side of x_c, the RPD function is robust against noise without AR. However, in the region $x < x_c$, the noise modifies the RPD. For $x < x_c$, the RPD approaches to uniform reinjection when noise is considered, at least locally around the unstable fixed point $x_0 = 0$.

Following reference [35], we obtained an analytical expression for the noisy reinjection probability density, NRPD. The noiseless density $\phi(x)$ transforms in a new density $\Phi(x)$ according to the convolution integral (see Fig. 4):

$$\Phi(x) = \int \phi(y) G(x - y, \sigma)\, \mathrm{d}y \tag{13}$$

where $G(x, \sigma)$ is the probability density of the noise term $\sigma\xi_n$ in Eq. (13). A random variable ξ in the interval $[-1, 1]$ is used as a noise source, and its probability density G results:

$$G(x, \sigma) = \frac{\Theta(x + \sigma) - \Theta(x - \sigma)}{2\sigma} \tag{14}$$

where $\Theta(x)$ is the Heaviside step function. If the function $\phi(x) = \lambda|x|^\alpha$ is introduced in the convolution integral, the resulting NRPD function is:

$$\Phi(x) = \frac{1}{c^{1+\alpha}} \frac{(|x| + \sigma)^{1+\alpha} - \mathrm{Sg}(|x| - \sigma)\ ||x| - \sigma|^{1+\alpha}}{2\sigma} \tag{15}$$

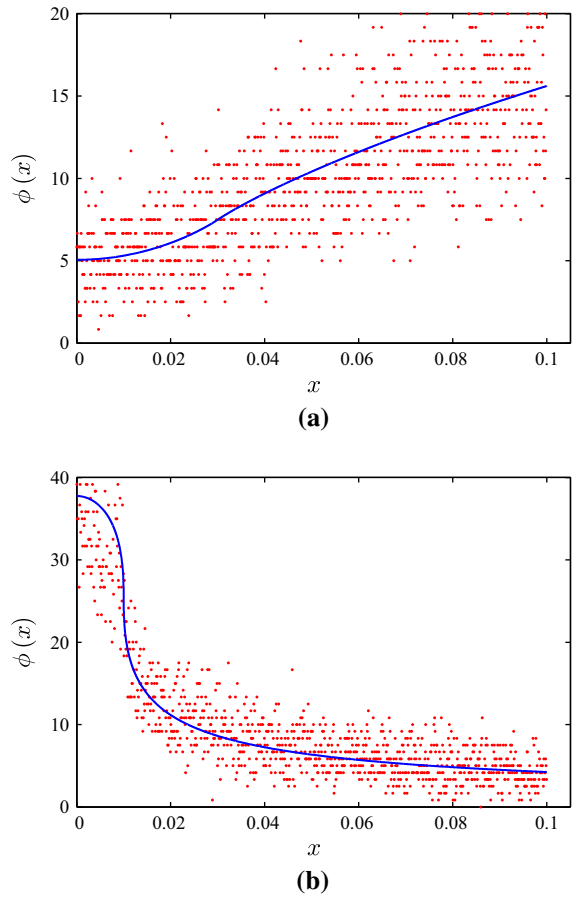

Fig. 6 NRPD for the map of Eq. (11)–(12). **a** $c = 0.1$, $\gamma = 0.65$, $\sigma = 0.03$ and **b** $c = 0.1$, $\gamma = 2$ and $\sigma = 0.01$. *Dots* correspond to numerical data, and the result of Eq. (15) is plotted as a *solid line*. (Color figure online)

where $\mathrm{Sg}(x)$ is the sign function.

In Fig. 6, we compare the NRPD calculated by Eq. (15) and the numerical simulation for different noise levels. The same values of m and α obtained from Fig. 5 are considered. Note the good agreement between the numerical and the analytical data.

4.2 Noisy RPD with AR and for LBR = 0

The noisy AR process cannot be neglected when all the effects on the reinjection probability function are considered. To obtain a full NRPD, we use the methodology described in the last sections. However, a more complex reinjection mechanism determines the function $M(x)$. Figures 7 and 8 show the functions $M(x)$

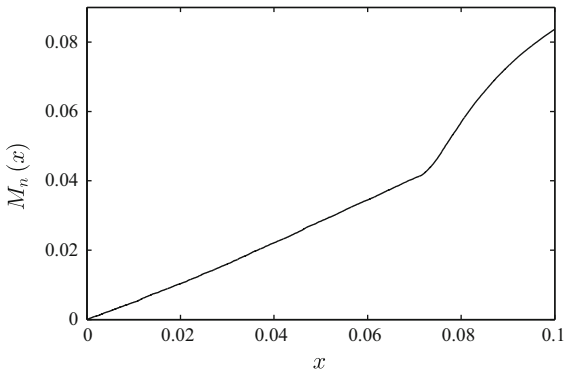

Fig. 7 Function $M(x)$ for $c = 0.1$, $\gamma = 0.65$, $\sigma = 0.03$ considering AR and for LBR $= 0$

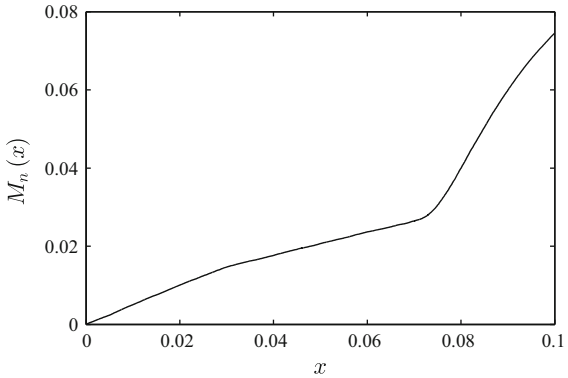

Fig. 8 Function $M_a(x)$ for $c = 0.1$, $\gamma = 2$, $\sigma = 0.03$ considering AR and for LBR $= 0$

for $c = 0.1$ and $\sigma = 0.03$ with $\gamma = 0.65$ and $\gamma = 2$, respectively. Both figures were calculated using 20,000 reinjected points. Similar figures are obtained for other values of c, γ and σ.

The figures show that the functions $M(x)$ have three zones: The first one starts at the fixed point and ends at $x = \sigma$, the second one is defined in the range $x = \sigma$ to $x = c - \sigma$, and the last one starts at $x = c - \sigma$ and ends at c. There are two points where $M(x)$ modifies its behavior (critical point): $x = \sigma$ and $x = c - \sigma$. In the previous subsection, we analyzed the change in the $M(x)$ behavior at point $x = \sigma$. Here, the AR, close to the upper limit of the laminar interval, c, produces a new modification of $M(x)$ in the interval $c - \sigma < x < c$.

To study the influence of the AR on the NRPD, a new function $M_a(x)$, using only the reinjected points inside the interval $c - \sigma < x < c$ is calculated. This function

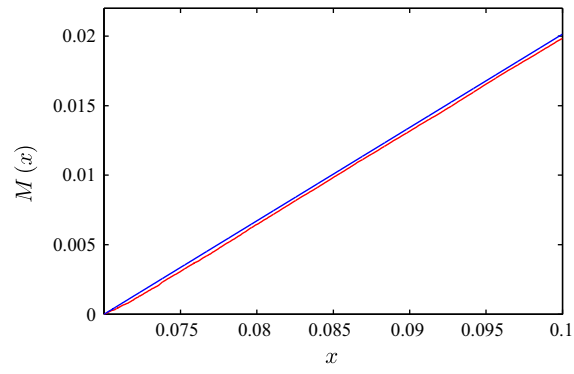

Fig. 9 Function $M_a(x)$ for $c = 0.1$, $\gamma = 2$, $\sigma = 0.03$ considering AR and for LBR $= 0$. (Color figure online)

has also a linear form. The slope of $M_a(x)$, m_a, gives the information required to calculate the exponent α_a to construct a local reinjection probability function $\phi_a(x)$, defined inside the interval $c - \sigma < x < c$:

$$\phi_a(x) = \lambda_a \left[x - (c - \sigma)\right]^{\alpha_a} \tag{16}$$

where

$$\alpha_a = \frac{2m_a - 1}{1 - m_a}, \qquad \lambda_a = \frac{\alpha_a + 1}{\sigma^{\alpha_a + 1}} \tag{17}$$

Equations (16) and (17) determine the new local NRPD produced by the noisy AR. Figure 9 shows $M_a(x)$ for $c - \sigma < x < c$ with $c = 0.1$, $\gamma = 2$ and $\sigma = 0.03$. The red and blue lines correspond to the numerical data and the minimal square interpolation, respectively. The slope, m_a, is approximately 1 ($m_a \approx 0.98$), corresponding to a uniform noise (see Eq. 14). Hence, we can observe that the AR governs the NRPD behavior inside the interval $(c - \sigma, c]$ because other reinjection mechanisms produce small effects on $\phi_a(x)$.

The NRPD is obtained using Eqs. (13) and (14) as shown in Eq. (18), where $(n - n_a)/n$ and $n_{a/n}$ are normalization parameters; n is the total number of reinjected points and n_a is the number of point reinjected into $(c - \sigma, c]$. For $x \leq (c - \sigma)$, Eq. (18) is similar to Eq. (15), i.e., the AR effect is not present in this subinterval. However, for $x > c - \sigma$, Eqs. (15) and (16) influence the NRPD.

$$\Phi_c(x) = \begin{cases} \left[\dfrac{1}{c^{1+\alpha}} \dfrac{(|x|+\sigma)^{1+\alpha} - \mathrm{Sg}(|x|-\sigma)||x|-\sigma|^{1+\alpha}}{2\sigma}\right]\left(\dfrac{n-n_a}{n}\right), & \text{if } x \le c-\sigma \\ \dfrac{1}{c^{1+\alpha}} \dfrac{(|x|+\sigma)^{1+\alpha} - \mathrm{Sg}(|x|-\sigma)||x|-\sigma|^{1+\alpha}}{2\sigma} \dfrac{n-n_a}{n} + \lambda_a \left[x-(c-\sigma)\right]^{\alpha_a} \dfrac{n_a}{n}, & \text{if } x > c-\sigma \end{cases} \tag{18}$$

$$\Phi_b(x) = \frac{1}{(c-x_s)^{1+\alpha}} \frac{(|x|+\sigma-x_s)^{1+\alpha} - \Theta(|x|-\sigma-x_s)||x|-\sigma-x_s|^{1+\alpha}}{2\sigma}, \tag{19}$$

$$\Phi_d(x) = \begin{cases} \dfrac{1}{c^{1+\alpha}} \dfrac{(|x|+\sigma-x_s)^{1+\alpha} + (|x-\sigma|-x_s)^{1+\alpha}}{2\sigma}, & \text{if } x < \sigma - x_s, \\ \dfrac{1}{c^{1+\alpha}} \dfrac{(|x|+\sigma-x_s)^{1+\alpha}}{2\sigma}, & \text{if } \sigma - x_s \le x < \sigma + x_s, \\ \dfrac{1}{c^{1+\alpha}} \dfrac{(|x|+\sigma-x_s)^{1+\alpha} - |(|x|-\sigma-x_s)|^{1+\alpha}}{2\sigma}, & \text{if } x \ge \sigma + x_s \end{cases} \tag{20}$$

$$\Phi_f(x) = \begin{cases} \Phi_b(x)\dfrac{n-n_a}{n}, & \text{if } x \le c-\sigma \\ \Phi_b(x) + \lambda_a (x-(c-\sigma))^{\alpha_a} \dfrac{n_a}{n}, & \text{if } x > c-\sigma \end{cases} \tag{21}$$

$$\Phi_f(x) = \begin{cases} \Phi_d(x)\dfrac{n-n_a}{n}, & \text{if } x \le c-\sigma \\ \Phi_d(x) + \lambda_a \left[x-(c-\sigma)\right]^{\alpha_a} \dfrac{n_a}{n}, & \text{if } x > c-\sigma \end{cases} \tag{22}$$

Figures 10 and 11 show the NRPD functions for the same parameters used in Figs. 7 and 8, respectively. The red points represent the numerical data and the blue lines the theoretical results calculated using Eq. (18). Both figures show an accurate agreement between numerical and analytical results.

4.3 Noisy RPD without AR and for LBR $\neq 0$

In this subsection, we study the LBR influence on the reinjection process without considering AR processes. If no restrictions are imposed over the noise strength (σ) and the LBR (x_s), two different cases can develop. One of them occurs when the noise intensity is lower than the LBR, $\sigma < x_s$. The other one occurs when the LBR is larger or equal than the noise intensity, $\sigma \le x_s$. When $\sigma < x_s$, the LBR changes due to noise. A "new LBR", depending on the original LBR and the noise strength, defined by the difference $x_i = x_s - \sigma$ will take place.

Figure 12 shows $M(x)$ for $\sigma < x_s$, $\varepsilon = 0.001$, $x_s = 0.05$, $\gamma = 2$, $c = 0.2$ and $\sigma = 0.03$ (20,000 reinjected points were used). We consider the same parameters

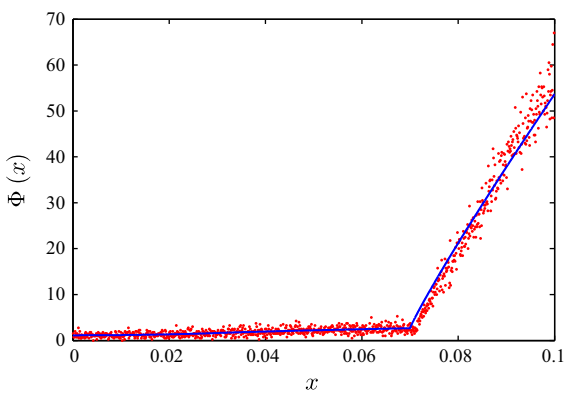

Fig. 10 NRPD function for $c = 0.1$, $\gamma = 0.65$, $\sigma = 0.03$ considering AR and for LBR $= 0$. (Color figure online)

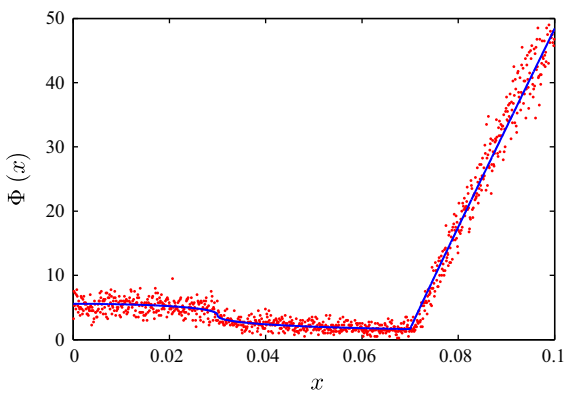

Fig. 11 NRPD function for $c = 0.1$, $\gamma = 2$, $\sigma = 0.03$ considering AR and for LBR $= 0$. (Color figure online)

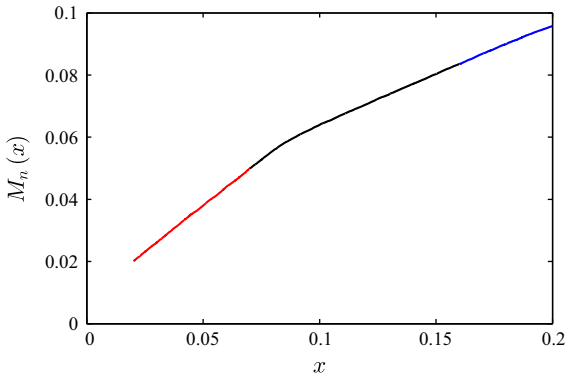

Fig. 12 Function $M(x)$. The parameters are $c = 0.2$, $\varepsilon = 10^{-3}$, $\sigma = 0.03$, $x_s = 0.05$, $\gamma = 2$. (Color figure online)

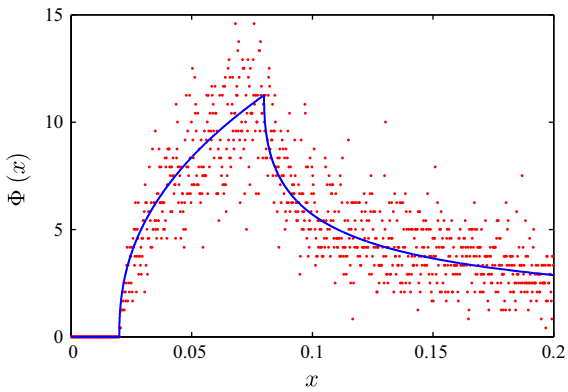

Fig. 13 NRPD function. The parameters are: $c = 0.2$, $\varepsilon = 10^{-3}$, $\sigma = 0.03$, $x_s = 0.05$, $\gamma = 2$. (Color figure online)

that Fig. 8, except for c and x_s. Note the two different slope behaviors of $M(x)$, m_l and m_r, separated by the point $x_c = x_s + \sigma = 0.8$, corresponding to the intervals $[x_s - \sigma, x_s + \sigma)$ and $[x_s + \sigma, c]$, respectively. The slope of the interval $[x_s + \sigma, c]$ is similar to the slope of the reinjection process without noise. To obtain these slopes, we use points of the intervals located not close to the singular point, $x_s + \sigma$. The red and blue lines indicate the points used to calculate the slopes in both intervals. For the test shown in Fig. 12, $m_l \approx 0.59$ ($\alpha_l \approx 0.45$) and $m_r \approx 0.303$ ($\alpha_r \approx -0.57$). In the noiseless case $m \approx 0.315$ and $\alpha \approx -0.541$.

By using Eq. (13), where α is the noiseless exponent of the RPD, we get the NRPD given by Eq. (19), where $\Theta(x)$ is the Heaviside step function. The numerical and theoretical NRPD functions, for the same parameters used in the previous figure, are shown in Fig. 13. The red points represent the numerical data, and the blue line is obtained using Eq. (19). Note that the analytical results accurately adjust the numerical data. The figure shows two different behaviors for the NRPD separated by the singular point $x_s + \sigma$. For one behavior, inside the interval $[x_s - \sigma, x_s + \sigma]$, the noise strongly influences the reinjection process. The second behavior occurs inside the interval $(x_s + \sigma, c]$. Similarly as $M(x)$, at the singular point, the NRPD behavior changes. Unlike the case with LBR $= 0$, the reinjection is not uniform around the unstable fixed point because there is no reinjection from negative x (see Eq. 12), thus, there is no symmetric reinjection for $\sigma < x_s$.

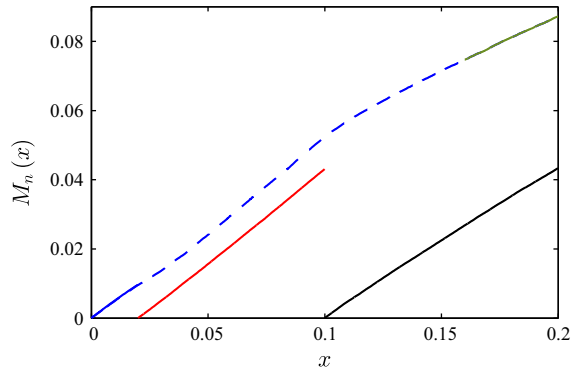

Fig. 14 Function $M(x)$. The parameters are: $c = 0.2$, $\varepsilon = 0.001$, $\sigma = 0.06$, $x_s = 0.04$. (Color figure online)

When $\sigma \geq x_s$ we can point out some differences respect to the previous analysis. One of them is due to the negative sign of the modified LBR, $x_i = x_s - \sigma$ producing a symmetric reinjection process which modifies the $M(x)$ and NRPD functions.

A test for $M(x)$ is presented in Fig. 14. The parameters are $\varepsilon = 0.001$, $x_s = 0.04$, $\gamma = 2$, $c = 0.2$ and $\sigma = 0.06$. This figure shows that $M(x)$ is split into three subintervals: $[0, \sigma - x_s)$, $[\sigma - x_s, \sigma + x_s)$ and $[\sigma + x_s, c]$ with two singular points, $\sigma - x_s$ and $\sigma + x_s$. If we only consider reinjection points inside each interval, the respective functions M_1, M_2 and M_3 are linear in each interval (see the blue, red and black continuous lines, respectively). The slope of $M_1(x)$ is $m_1 \approx 0.49$, converging to $1/2$ ($\alpha \to 0$). Note that $M_1(x) = M(x)$ inside the interval $[0, \sigma - x_s)$. Therefore, close to $x \approx 0$, the reinjection is uniform. This is possible due to the reinjection of negative x and also because the reinjection process is symmetric around $x = 0$. On the other hand, the slope of $M(x)$ close to c (see green continuous line) is $m_b \approx 0.3145$ ($\alpha \approx -0.54$), which is very close to the slope of the noiseless $M(x)$ ($m \approx 0.3145$).

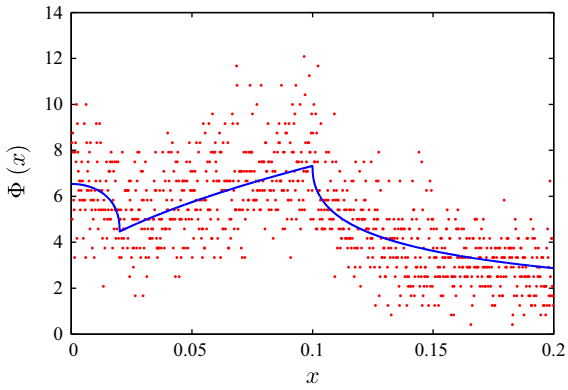

Fig. 15 NRPD function. The parameters are: $c = 0.2$, $\varepsilon = 10^{-3}$, $\sigma = 0.06$, $x_s = 0.04$. (Color figure online)

After solving Eq. (13), the theoretical NRPD is shown in Eq. (20), where α is the noiseless reinjection process and can be evaluated using the slope m_3 of the local function $M_3(x)$ inside the interval $[\sigma + x_s, c]$. Similarly to what happens with $M(x)$, the NRPD function has two singular points and three behaviors inside the laminar interval.

Figure 15 shows the NRPD for the same parameters used in Fig. 14. The blue line corresponds to the theoretical evaluation, and the numerical data are given by red points. The agreement between analytical and numerical NRPD is very good.

4.4 Noisy RPD with a LBR $\neq 0$ and AR

We can now study the influence of both, the LBR and the AR on the NRPD function. If the full noise effects on the reinjection probability function are considered, the noisy AR process should be taken into consideration.

Similarly to the analysis of the previous subsection, two different cases can arise, one for $\sigma < x_s$, and the other one for $\sigma \geq x_s$. Figure 16 shows $M(x)$ for the cases verifying $\sigma < x_s$, with $c = 0.2$, $\varepsilon = 0.001$, $\sigma = 0.03$, $x_s = 0.05$ and $\gamma = 2$. The function $M(x)$ has different behaviors in the three intervals $[x_s - \sigma, x_s + \sigma)$, $[x_s + \sigma, c - \sigma)$ and $[c - \sigma, c]$. For $[x_s - \sigma, x_s + \sigma)$ and $[x_s + \sigma, c - \sigma)$, $M(x)$ behaves as described in the previous subsection; whereas for $[c - \sigma, c]$, $M(x)$ is defined by the AR process. Similar figures are obtained for other control parameters.

The full NRPD for $\sigma < x_s$ is obtained integrating Eq. (13), which is shown in Eq. (21), where $(n - n_a)/n$ and n_a/n are normalization parameters, being n the total number of reinjected points and n_a the number of reinjected points considering the AR mechanism. Figure 17 shows the numerical data and the analytical results evaluated using Eq. (15) for $c = 0.2$, $\varepsilon = 0.001$, $\sigma = 0.03$, $x_s = 0.05$ and $\gamma = 2$. The NRPD is discontinuous and divided in three subintervals. Despite this specific behavior, note the accuracy of the theoretical results with the numerical ones.

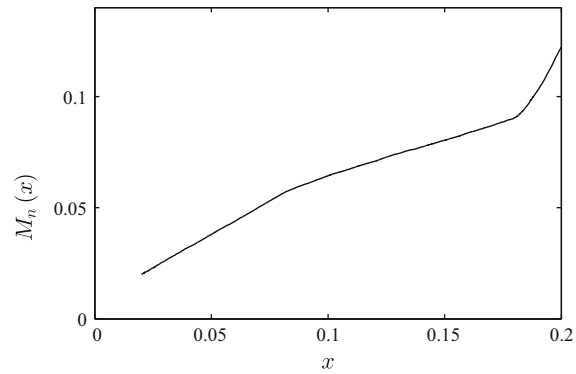

Fig. 16 Function $M(x)$. The parameters are: $c = 0.2$, $\varepsilon = 0.001$, $\sigma = 0.03$, $x_s = 0.05$ and $\gamma = 2$

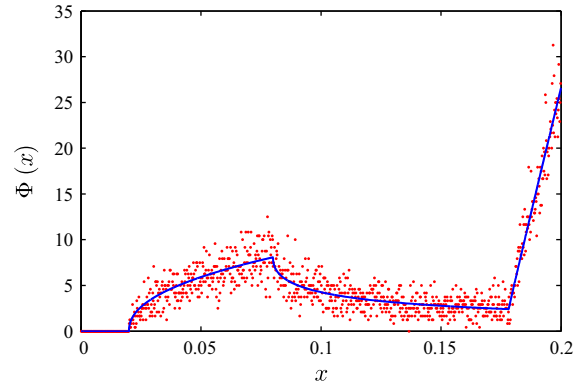

Fig. 17 NRPD function considering all effects. The parameters are $c = 0.2$, $\varepsilon = 0.001$, $\sigma = 0.03$, $x_s = 0.05$ and $\gamma = 2$. (Color figure online)

Now the cases verifying $\sigma \geq x_s$ are studied. $M(x)$ is calculated using Eq. (2). Figure 18 shows the function $M(x)$, for $c = 0.2$, $\varepsilon = 0.001$, $\sigma = 0.06$, $x_s = 0.03$ and $\gamma = 2$, with four different behaviors corresponding to the four intervals $[0, x_s - \sigma)$, $[x_s - \sigma, x_s + \sigma)$, $[x_s + \sigma, c - \sigma)$ and $[c - \sigma, c]$. For the three intervals $[0, x_s - \sigma)$, $[x_s - \sigma, x_s + \sigma)$ and $[x_s + \sigma, c - \sigma)$ the function $M(x)$ has a similar behavior as those described in the previous subsection. For the interval $[c - \sigma, c]$, $M(x)$ is defined by the AR process.

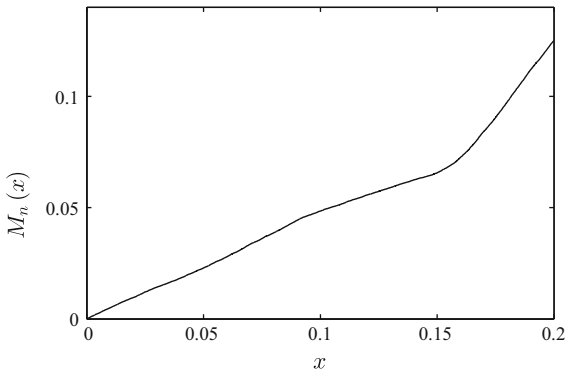

Fig. 18 $M(x)$ for parameters: $c = 0.2$, $\varepsilon = 0.001$, $\sigma = 0.06$, $x_s = 0.03$ and $\gamma = 2$

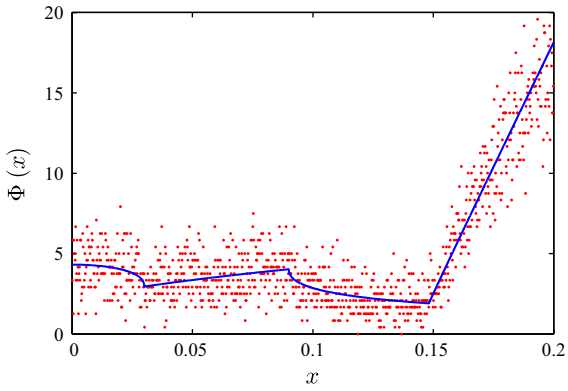

Fig. 19 NRPD function considering all effects. The parameters are: $c = 0.2$, $\varepsilon = 0.001$, $\sigma = 0.06$, $x_s = 0.06$, $\gamma = 2$. (Color figure online)

The full NRPD function for $\sigma \geq x_s$ can be calculated using the convolution integral Eq. (13), which is shown in Eq. (22). The full NRPD is shown in Fig. 19. This figure shows that the analytical results (blue lines) obtained using Eq. (22) for $c = 0.2$, $\varepsilon = 0.001$, $\sigma = 0.06$, $x_s = 0.03$ and $\gamma = 2$, are in good agreement with the numerical data (red symbols). In addition, it can also be observed that the NRPD is divided in four subintervals as the function $M(x)$.

5 Probability density of the laminar lengths

We are interested in the study of the probability density of the laminar lengths, $\Phi_l(l)$, considering the effect of the LBR and noise for two cases: (1) when the noise intensity is lower than the LBR, $\sigma < x_s$ and (2) when the noise intensity is equal or larger than the LBR, $x_s \geq \sigma$. For the two cases, we consider two alternatives: with and without AR.

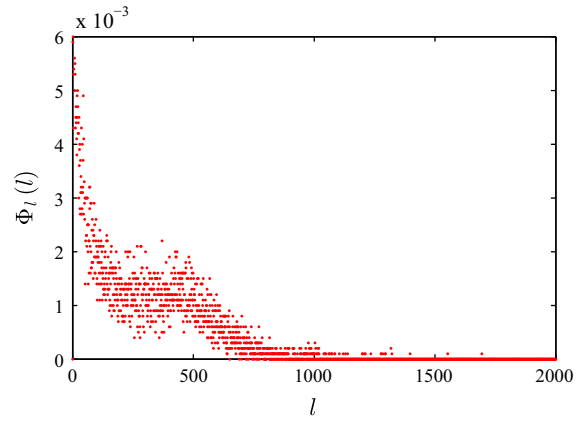

Fig. 20 Probability density of the laminar lengths considering noise for σ close to ε. The parameters are $c = 0.1$, $\varepsilon = 0.001$, $\sigma = 0.0005$, $x_s = 0.02$, $\gamma = 2$ and $p = 3$

5.1 Probability density of the laminar lengths for $\sigma < x_s$ without AR

We study three different cases depending on the relation between the noise intensity, σ, and the control parameter ε: (1) $\sigma \ll \varepsilon$; (2) σ is close to ε and (3) $\sigma \gg \varepsilon$.

For $\sigma \ll \varepsilon$, the noise has not much influence on the reinjection process; the probability density of the laminar lengths is not modified by noise and the shape of $\Phi_l(l)$ is as in Fig. 3.

When the noise intensity σ is close to ε, the noise modifies the reinjection mechanism and the probability density of the laminar lengths is affected. Figure 20 shows $\Phi_l(l)$ for the same set of parameters that Fig. 3, except $\sigma = 0.0005$. Unlike Fig. 3, in Fig. 20, there is not a cutoff and larger laminar lengths appear. Also, close to the noiseless cutoff, $\Phi_l(l)$ becomes larger.

When $\sigma \gg \varepsilon$, noise governs the reinjection process and $\Phi_l(l)$ is modified. In Fig. 21, we increase σ up to 0.001 Note that $\Phi_l(l)$ decreases with l and larger values of the laminar length arise. A similar behavior for type-I intermittency was described in [40].

5.2 Probability density of the laminar lengths for $\sigma < x_s$ with AR

Similar to the previous analysis, in this study there are three possible cases: (1) $\sigma \ll \varepsilon$; (2) σ is close to ε and (3) $\sigma \gg \varepsilon$. Figure 22 shows the probability density of the laminar lengths for $c = 0.1$, $\varepsilon = 0.001$, $\sigma = 0.0001$, $x_s = 0.02$, $\gamma = 2$ and $p = 3$ when AR is

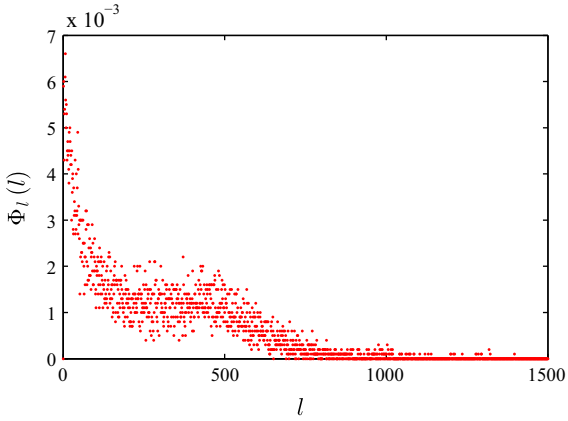

Fig. 21 Probability density of the laminar lengths considering noise for $\sigma \gg \varepsilon$. The parameters are $c = 0.1$, $\varepsilon = 0.001$, $\sigma = 0.01$, $x_s = 0.02$, $\gamma = 2$ and $p = 3$

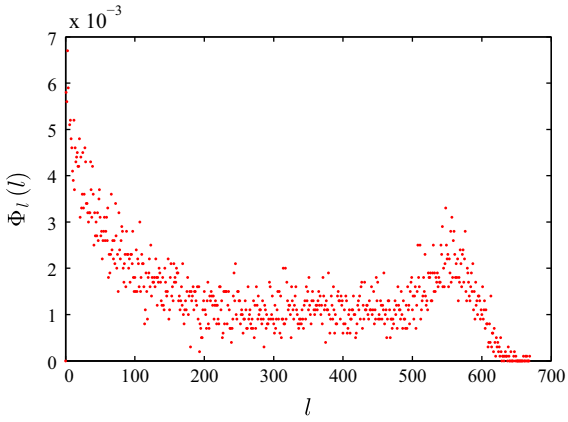

Fig. 22 Probability density of the laminar lengths with noise $\sigma \ll \varepsilon$ and AR. The parameters are: $c = 0.1$, $\varepsilon = 0.001$, $\sigma = 0.0001$, $x_s = 0.02$, $\gamma = 2$, $p = 3$

considered. The function $\Phi_l(l)$ has a different behavior than in Fig. 3 (without noise) and is also different that the case with noise and without AR (see Fig. 20). It should be noted that there is not a cutoff, instead there is an increment of $\Phi_l(l)$. Also, the largest laminar length is not significantly increased because the trajectories have mostly short laminar lengths, due to the fact that they are reinjected by the adjacent reinjection process.

When the noise intensity σ is close to ε, the noise strongly modifies the reinjection mechanism, accordingly, $\Phi_l(l)$ is similar to that shown in Fig. 21. Figure 23 shows $\Phi_l(l)$ for $c = 0.1$, $\varepsilon = 0.001$, $\sigma = 0.0005$, $x_s = 0.02$, $\gamma = 2$ and $p = 3$.

When $\sigma \gg \varepsilon$ the AR has a strong influence on $\Phi_l(l)$. Figure 24 shows the probability density of the laminar

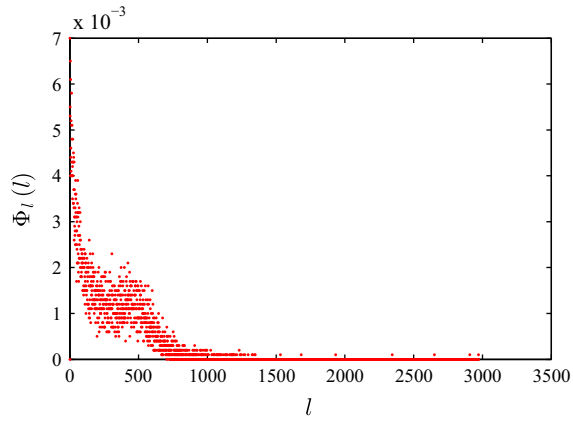

Fig. 23 Probability density of the laminar lengths considering noise when σ is close to ε. The parameters are: $c = 0.1$, $\varepsilon = 0.001$, $\sigma = 0.0005$, $x_s = 0.02$, $\gamma = 2$ and $p = 3$

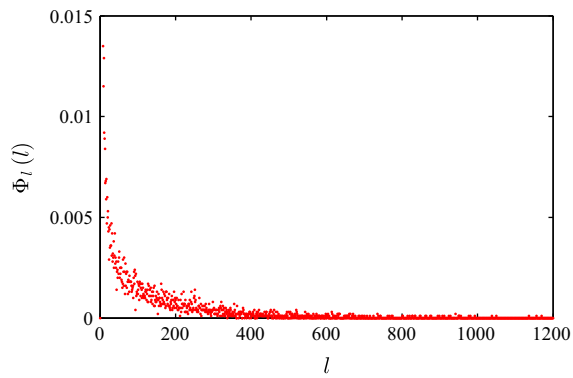

Fig. 24 Probability density of the laminar lengths considering noise for $\sigma \gg \varepsilon$ and AR. The parameters are: $c = 0.1$, $\varepsilon = 0.001$, $\sigma = 0.01$, $x_s = 0.02$, $\gamma = 2$ and $p = 3$

lengths for $c = 0.1$, $\varepsilon = 0.001$, $\sigma = 0.01$, $x_s = 0.02$, $\gamma = 2$ and $p = 3$. Note that $\Phi_l(l)$ has a large concentration near $l = 0$, which is produced by the AR mechanism because the reinjected points need short time to exit the laminar interval.

5.3 Probability density of the laminar lengths for $\sigma \geq x_s$

When $\sigma \geq x_s$ the only significant case is given by $\sigma \gg \varepsilon$. For $\sigma \leq \varepsilon$, the LBR is very small and it is infinitely close to the fixed point. Figure 25 shows the function $\Phi_l(l)$ with and without AR. The parameters used are $c = 0.1$, $\varepsilon = 0.001$, $\sigma = 0.03$, $x_s = 0.02$, $\gamma = 2$ and $p = 3$. The blue and red symbols correspond to the case with and without AR. When the noise inten-

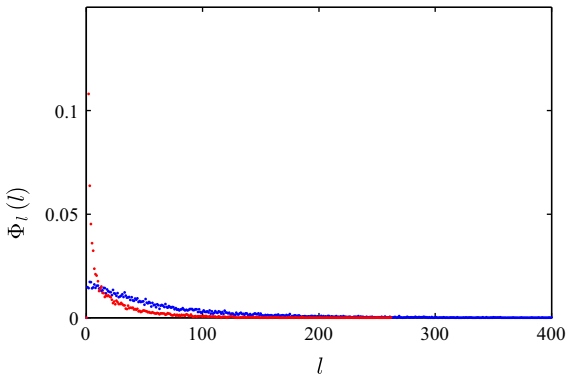

Fig. 25 Probability density of the laminar lengths considering noise for $\sigma \gg \varepsilon$ and AR. The parameters are: $c = 0.1$, $\varepsilon = 0.001$, $\sigma = 0.03$, $x_s = 0.02$, $\gamma = 2$ and $p = 3$. The *red* and the *blue symbols* correspond to the cases with and without AR, respectively. (Color figure online)

sity is considerably larger than the control parameter ε the noise governs the reinjection process, and $\Phi_l(l)$ loses its original behavior (see the red symbols). However, when AR is considered, the maximum length is reduced and a high concentration close to $l \to 0$ is observed.

6 Conclusions

In this work, some recent studies proposed in [32,35,36] were extended to consider type-II intermittency with nonzero lower boundary of reinjection and high noise intensity. We studied the influence of σ and the LBR value on the reinjection probability density as well as the probability density of the laminar lengths. Also, the effect produced by the adjacent reinjection mechanism is evaluated.

To carry out this study, we used the auxiliary function $M(x)$ that is easier to calculate than the RPD. We found that the laminar interval can be split in subintervals in which the function $M(x)$ preserves the linear form. By means of this methodology, it was possible to calculate the noisy RPD function, which is represented by functions with discontinuous first derivatives. In the all tests, the numerical data and the theoretical results showed a very good agreement. On the other hand, we note that using the NRPD, evaluated from noisy data, we can obtain a complete description of the noiseless system.

The adjacent reinjection concept was introduced, and its effects on the RPD were analyzed. This mechanism produces a high reinjection concentration near the upper limit of the laminar interval; and it is more noticeable for increasing noise intensity.

For $\sigma = 0$ and LBR $\neq 0$, the probability density of the laminar lengths presents a cutoff. However, for $\sigma \neq 0$ the cutoff disappears, and long laminar lengths can exist. Finally, note that the theoretical formulation that we present here does not impose restrictions on the relation between the noise intensity, σ and the control parameter ε.

Acknowledgments This research was supported by CONICET, National University of Córdoba and MCyT of Córdoba of Argentina, and the Ministerio de Economía y Competitividad of Spain under Grant ESP2013-41078-R.

References

1. Manneville, P., Pomeau, Y.: Intermittency and Lorenz model. Phys. Lett. A **75**, 1–2 (1979)
2. Manneville, P.: Intermittency, self-similarity and $1/f$ spectrum in dissipative dynamical systems. Le Journal de Physique **41**, 1235–1243 (1980)
3. Schuster, H., Just, W.: Deterministic Chaos. Wiley VCH, Mörlenbach (2005)
4. Nayfeh, A., Balachandran, B.: Applied Nonlinear Dynamics. Wiley, New York (1995)
5. Marek, M., Schreiber, I.: Chaotic Behaviour of Deterministic Dissipative Systems. Cambridge University Press, Cambridge (1995)
6. Kaplan, H.: Return to type-I intermittency. Phys. Rev. Lett. **68**, 553–557 (1992)
7. Price, T., Mullin, P.: An experimental observation of a new type of intermittency. Physica D **48**, 29–52 (1991)
8. Platt, N., Spiegel, E., Tresser, C.: On-off intermittency: a mechanism for bursting. Phys. Rev. Lett. **70**, 279–282 (1993)
9. Pikovsky, A., Osipov, G., Rosenblum, M., Zaks, M., Kurths, J.: Attractor-repeller collision and eyelet intermittency at the transition to phase synchronization. Phys. Rev. Lett. **79**, 47–50 (1997)
10. Lee, K., Kwak, Y., Lim, T.: Phase jumps near a phase synchronization transition in systems of two coupled chaotic oscillators. Phys. Rev. Lett. **81**, 321–324 (1998)
11. Hramov, A., Koronovskii, A., Kurovskaya, M., Boccaletti, S.: Ring intermittency in coupled chaotic oscillators at the boundary of phase synchronization. Phys. Rev. Lett. **97**, 114101 (2006)
12. Stavrinides, S., Anagnostopoulos, A.: The route from synchronization to desynchronization of chaotic operating circuits and systems. In: Banerjee, S., Rondoni, L. (eds.) Chapter 9, in Applications of Chaos and nonlinear dynamics in science and engineering. Springer-Verlag, Berlin (2013)
13. Dubois, M., Rubio, M., Berge, P.: Experimental evidence of intermittencies associated with a subharmonic bifurcation. Phys. Rev. Lett. **16**, 1446–1449 (1983)

14. Malasoma, J., Werny, P., Boiron, M.: Multichannel type-I intermittency in two models of Rayleigh–Benard convection. Phys. Rev. Lett. **51**, 487–500 (2004)
15. Stavrinides, S., Miliou, A., Laopoulos, T., Anagnostopoulos, A.: The intermittency route to chaos of an electronic digital oscillator. Int. J. Bifurcat. Chaos **18**, 1561–1566 (2008)
16. Sanmartin, J., Lopez-Rebollal, O., del Rio, E., Elaskar, S.: Hard transition to chaotic dynamics in Alfven wave-fronts. Phys. Plasmas **11**, 2026–2035 (2004)
17. Sanchez-Arriaga, G., Sanmartin, J., Elaskar, S.: Damping models in the truncated derivative nonlinear Schrödinger equation. Phys. Plasmas **14**, 082108 (2007)
18. Pizza, G., Frouzakis, C., Mantzaras, J.: Chaotic dynamics in premixed Hydrogen/air channel flow combustion. Combust. Theor. Model. **16**, 275–299 (2012)
19. Nishiura, Y., Ueyama, D., Yanagita, T.: Chaotic pulses for discrete reaction diffusion systems. SIAM J. Appl. Dyn. Syst. **4**, 723–754 (2005)
20. de Anna, P., Le Borgne, T., Dentz, M., Tartakovsky, A., Bolster, D., Davy, P.: Flow intermittency, dispersion and correlated continuous time random walks in porous media. Phys. Rev. Lett. **110**, 184502 (2013)
21. Stan, C., Cristescu, C., Dimitriu, D.: Analysis of the intermittency behavior in a low-temperature discharge plasma by recurrence plot quantification. Phys. Plasmas **17**, 042115 (2010)
22. Chian, A.: Complex System Approach to Economic Dynamics. Lecture Notes in Economics and Mathematical Systems, pp. 39–50. Springer, Berlin (2007)
23. Zebrowski, J., Baranowski, R.: Type-I intermittency in nonstationary systems: models and human heart-rate variability. Physica A **336**, 74–86 (2004)
24. Paradisi, P., Allegrini, P., Gemignani, A., Laurino, M., Menicucci, D., Piarulli, A.: Scaling and intermittency of brains events as a manifestation of consciousness. AIP Conf. Proc. **1510**, 151–161 (2012)
25. Baptista, M., Caldas, I.: Dynamics of the two-frequency torus breakdown in the driven double scroll circuit. Phys. Rev. E **58**, 4413–4420 (1998)
26. Baptista, M., Caldas, I.: Type-II intermittency in the driven double scroll circuit. Physica A **132**, 325–338 (1999)
27. Kim, M., Lee, H., Kim, C., Pang, H., Lee, E., Known, O.: New characteristic relations in type-II and III intermittency. Int. J. Bifurcat. Chaos **7**, 831–836 (1998)
28. Hirsch, E., Huberman, B., Scalapino, D.: Theory of intermittency. Phys. Rev. A **25**, 519–532 (1982)
29. Koronovskii, A., Hramov, A.: Type-II intermittency characteristics in the presence of noise. Eur. Phys. J. B **62**, 447–452 (2008)
30. Kye, W., Rim, S., Kim, C., Lee, J., Ryu, J., Yeom, B., Park, Y.: Experimental observation of characteristic relations of type-III intermittency in the presence of noise in a simple electronic circuit. Phys. Rev. E **68**, 036203 (2003)
31. Wiggins, S.: Introduction to Applied Nonlinear Dynamical Systems and Chaos. Springer, Berlin (2003)
32. del Rio, E., Elaskar, S.: New characteristic relation in type-II intermittency. Int. J. Bifurcat. Chaos **20**, 1185–1191 (2010)
33. Kye, W., Kim, C.: Characteristic relations of type-I intermittency in presence of noise. Phys. Rev. E **62**, 6304–6307 (2000)
34. Elaskar, S., del Rio, E., Donoso, J.: Reinjection probability density in type-III intermittency. Physica A **390**, 2759–2768 (2011)
35. del Rio, E., Sanjuan, M., Elaskar, S.: Effect of noise on the reinjection probability density in intermittency. Commun. Nonlinear Sci. Numer. Simul. **17**, 3587–3596 (2012)
36. Elaskar, S., del Rio, E.: Intermittency reinjection probability function with and without noise effects. Latest Trends in Circuits, Automatics Control and Signal Processing, pp. 145–154, ISBN: 978-1-61804-131-9, Barcelona (2012)
37. del Rio, E., Elaskar, S., Makarov, S.: Theory of intermittency applied to classical pathological cases. Chaos **23**, 033112 (2013)
38. del Rio, E., Elaskar, S., Donoso, J.: Laminar length and characteristic relation in type-I intermittency. Commun. Nonlinear Sci. Numer. Simul. **19**, 967–976 (2014)
39. Krause, G., Elaskar, S., del Rio, E.: Type-I intermittency with discontinuous reinjection probability density in a truncation model of the derivative nonlinear Schrödinger equation. Nonlinear Dyn. **77**, 455–466 (2014)
40. Krause, G., Elaskar, S., del Rio, E.: Noise effect on statistical properties of type-I intermittency. Physica A **402**, 318–329 (2014)